

Pressure-induced transition from the dynamic to static Jahn-Teller effect in $(\text{Ph}_4\text{P})_2\text{ICl}_6$

Estaline Amitha Francis, S. Scharinger, K. Németh, K. Kamarás,
Christine A. Kuntscher

Angaben zur Veröffentlichung / Publication details:

Francis, Estaline Amitha, S. Scharinger, K. Németh, K. Kamarás, and Christine A. Kuntscher. 2012. "Pressure-induced transition from the dynamic to static Jahn-Teller effect in $(\text{Ph}_4\text{P})_2\text{ICl}_6$." *Physical Review B* 85 (19): 195428.
<https://doi.org/10.1103/physrevb.85.195428>.



Pressure-induced transition from the dynamic to static Jahn-Teller effect in $(\text{Ph}_4\text{P})_2\text{IC}_{60}$

E. A. Francis,¹ S. Scharinger,¹ K. Németh,² K. Kamarás,² and C. A. Kuntscher^{1,*}

¹*Experimentalphysik 2, Universität Augsburg, D-86135 Augsburg, Germany*

²*Institute for Solid State Physics and Optics, Wigner Research Centre for Physics, Hungarian Academy of Sciences, P. O. Box 49, H-1525 Budapest, Hungary*

(Received 19 March 2012; published 14 May 2012)

High-pressure infrared transmission measurements on $(\text{Ph}_4\text{P})_2\text{IC}_{60}$ were performed up to 9 GPa over a broad frequency range (200–20000 cm^{-1}) to monitor the vibrational and electronic/vibronic excitations under pressure. The four fundamental T_{1u} modes of C_{60}^- are split into doublets already at the lowest applied pressure and harden with increasing pressure. Several cation modes and fullerene-related modes split into doublets at around 2 GPa, the most prominent one being the G_{1u} mode. The splitting of the vibrational modes can be attributed to the transition from the dynamic to static Jahn-Teller effect, caused by steric crowding at high pressure. Four absorption bands are observed in the NIR-visible frequency range. They are discussed in terms of transitions between LUMO electronic states in C_{60}^- , which are split because of the Jahn-Teller distortion and can be coupled with vibrational modes. Various distortions and the corresponding symmetry lowering are discussed. The observed redshift of the absorption bands indicates that the splitting of the LUMO electronic states is reduced upon pressure application.

DOI: [10.1103/PhysRevB.85.195428](https://doi.org/10.1103/PhysRevB.85.195428)

PACS number(s): 78.30.Na, 71.70.Ej, 33.20.Ea, 33.20.Wr

I. INTRODUCTION

Tetraphenylphosphonium iodide- C_{60} [$(\text{Ph}_4\text{P})_2\text{IC}_{60}$] is a prototype to study C_{60}^- radical anion in a solid state environment, as large cations $(\text{Ph}_4\text{P})_2\text{I}$ are so well positioned that they separate the C_{60} ions from each other (see Fig. 1). The weak coupling between the C_{60}^- and the $(\text{Ph}_4\text{P}^+)X^-$ structural units was demonstrated by Raman measurements on $(\text{Ph}_4\text{P})_2\text{C}_{60}X$ ($X = \text{Cl}, \text{Br}, \text{I}$) showing the insensitivity of the spectra to the halogen anion.¹ The compounds $(\text{Ph}_4\text{P})_2\text{C}_{60}X$ have the advantage of being air stable unlike the other fullerides. Also they can be grown as single crystals in contrast to the powder form of several other fullerides. $(\text{Ph}_4\text{P})_2\text{IC}_{60}$ crystallizes in a tetragonal structure with the space group $I4/m$.^{2–4} At room temperature, the dynamic nature of the Jahn-Teller (JT) effect in $(\text{Ph}_4Y)_2XC_{60}$ ($Y = \text{P}$ or As , $X = \text{Cl}, \text{I}$, or Br) was shown by electron spin resonance (ESR), nuclear magnetic resonance (NMR), and infrared (IR) spectroscopy.^{5–7}

Theoretically, the dynamic JT effect for singly charged fullerene C_{60}^- is expected to be reflected in the IR spectrum. At room temperature, the dynamic disorder between different orientations of the C_{60}^- is signaled in the infrared spectrum by the splitting of the T_{1u} fundamental modes of fullerene and the activation of silent modes. Neutral C_{60} possesses the highest I_h symmetry with 174 possible vibration modes, out of which only four T_{1u} modes are infrared active due to symmetry considerations. The temperature dependence of the JT dynamics was studied on these compounds by far-infrared spectroscopy.^{5–12}

Another experimental evidence for the dynamic nature of the JT effect in $(\text{Ph}_4\text{P})_2\text{IC}_{60}$ was obtained by ESR,^{8–12} namely by the splitting of the LUMO of C_{60}^- above 40 K through an Orbach spin-lattice relaxation process.¹⁰ The ESR results¹² on $[A^+(\text{C}_6\text{H}_5)_4]_2\text{C}_{60}^-B^-$ (where $A = \text{P}$ or As and $B = \text{I}$ or Cl) indicate static disorder with random occupation of two “standard orientations” at low temperature. Ordering phenomena were also found in x-ray diffuse scattering and diffraction measurements: Launois *et al.*¹³ found evidence for a structural phase transition in $(\text{Ph}_4\text{P}^+)_2\text{C}_{60}^- \text{Br}^-$ at around 120 K during

cooling down, where the C_{60} molecules show an orientational order with the formation of two types of orientational domains. Simultaneously, the average crystal structure is changed from $I4/m$ to $I2/m$, and the related lowering of the crystal field symmetry leads to a static stabilization of the JT distortion of the C_{60}^- molecule.¹³ This scenario is consistent with the results of far-infrared transmission measurements, which revealed a weak transition in the range 125–150 K.⁵ Later on, based on x-ray diffraction data² a glass transition was proposed to occur in $(\text{Ph}_4\text{As})_2\text{ClC}_{60}$ at 125 K, where the dynamic disorder of the C_{60} molecules over two orientations becomes static. Besides, an upper bound of 0.01 Å for the JT distortion of the C_{60} molecules was established.²

The goal of this work was to study the pressure-induced effects in $(\text{Ph}_4\text{P})_2\text{IC}_{60}$ in detail, as compared to earlier investigations,¹⁴ and to compare them to those induced by temperature decrease. The interesting similarity between the temperature lowering and increasing pressure is exhibited by C_{60} and several fullerene-based compounds.^{15–17} In the case of $(\text{Ph}_4\text{P})_2\text{IC}_{60}$, temperature lowering causes a decrease of the lattice constants and the decreasing thermal energy induces a dynamic-to-static JT transition. In comparison, generally the increase in pressure reduces lattice constants but does not change the thermal energy of the system. Hence, the changes of the nature of the JT effect do not necessarily need to be similar during temperature lowering and pressure increase. The goal of this infrared study was to compare the effects of pressure versus temperature lowering on the vibration properties and the electronic and vibronic excitations in $(\text{Ph}_4\text{P})_2\text{IC}_{60}$.

We present the results of high-pressure infrared studies on $(\text{Ph}_4\text{P})_2\text{IC}_{60}$ up to 9 GPa over a broad frequency range between 300–20000 cm^{-1} . As the time scale of infrared measurements (10^{-11} s⁻¹) is of the order of the JT pseudorotation frequency of the C_{60}^- ion, IR spectroscopy is a powerful tool to investigate the JT dynamics. We can address the symmetry changes of the molecule as a function of pressure. Investigating the electronic transitions of the C_{60}^- anion can help to understand the intermolecular interactions, charge transfer process, and

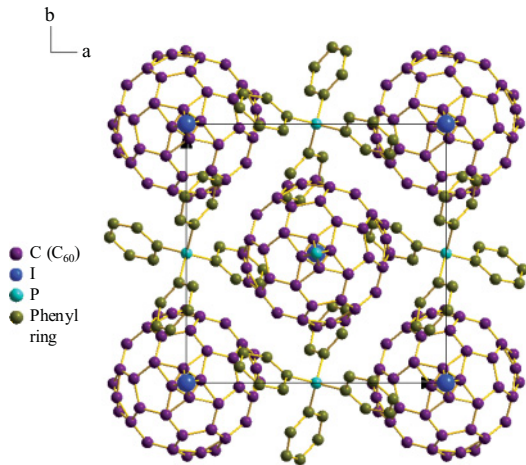


FIG. 1. (Color online) Crystal structure of $(\text{Ph}_4\text{P})_2\text{IC}_{60}$ (Refs. 2–4).

electronic states. For example, it was proposed that the halogen anion radius changes the charge distribution on C_{60}^- , which may alter its vibrational characteristics and electronic absorption.¹⁸ The pressure dependence of the vibrational and electronic properties of $(\text{Ph}_4\text{P})_2\text{IC}_{60}$ are thus studied in detail.

II. EXPERIMENT

A. Synthesis of $(\text{Ph}_4\text{P})_2\text{IC}_{60}$ crystals

Small single crystals of $(\text{Ph}_4\text{P})_2\text{IC}_{60}$ were grown by electrocrystallization over platinum cathode with a constant current of $30 \mu\text{A}$. Electrolysis was carried out in the solution of Ph_4PI and C_{60} dissolved in 1:1 mixture of dichloromethane and toluene at ambient conditions.¹⁹ Black shiny crystals of $100\text{--}300 \mu\text{m}$ size [see Fig. 2(a)] were collected from the electrode after 5 days.

B. High-pressure infrared measurements

Infrared transmission measurements were carried out with an infrared microscope Bruker IR scope II with $15\times$ magnification coupled to a Bruker 66v/S Fourier transform infrared spectrometer. The high pressure was generated by a Syassen-Holzapfel diamond anvil cell (DAC)²⁰ equipped with type IIA diamonds suitable for infrared measurements. The ruby luminescence method was used for pressure determination.²¹ The transmission was measured for pressures up to 9 GPa between 200 cm^{-1} and 20000 cm^{-1} . Finely ground CsI was used as quasi-hydrostatic pressure transmitting medium. Data were collected with resolution of 1 cm^{-1} for $100\text{--}600 \text{ cm}^{-1}$, 2 cm^{-1} for $550\text{--}8000 \text{ cm}^{-1}$ frequency range. For the transmission measurements in the NIR-visible region a powder sample was mixed with CsI and filled in the DAC. Measurements were carried out with 4 cm^{-1} resolution in the NIR-visible region. All measurements were carried out at room temperature. A microscopic view of the DAC filled with samples, the pressure transmitting medium, and the ruby ball is shown in Fig. 2(b).

In order to determine the transmittance of $(\text{Ph}_4\text{P})_2\text{IC}_{60}$ under pressure, the intensity $I_s(\omega)$ of the radiation transmitted by the sample or by the mixture of the powder sample and the pressure transmitting medium was measured, as illustrated

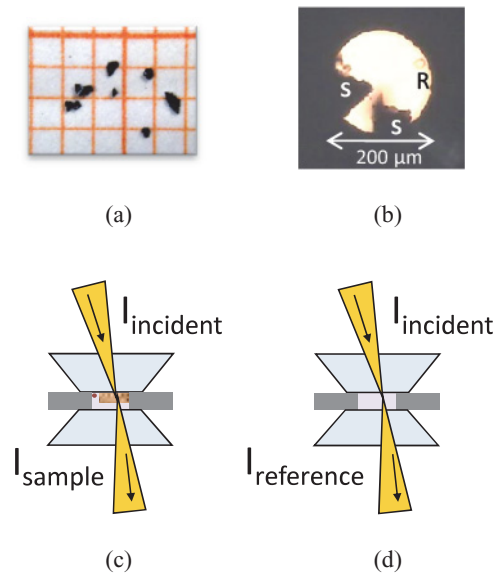


FIG. 2. (Color online) (a) Photo of $(\text{Ph}_4\text{P})_2\text{IC}_{60}$ single crystals on millimeter paper. (b) Microscopic view of the DAC filled with samples (S), ruby ball (R), and pressure-transmitting medium (bright area). Scheme of (c) the transmission through the sample, and (d) the transmission through the pressure-transmitting medium (CsI).

in Fig. 2(c). As reference, the intensity $I_r(\omega)$ transmitted by the pressure transmitting medium inside the DAC was used, as shown in Fig. 2(d). The transmittance was then calculated according to $T(\omega) = I_s(\omega)/I_r(\omega)$ and the absorbance is given by $A = \log_{10}(1/T)$.

III. RESULTS AND DISCUSSION

A. Assignment of excitations at lowest pressure

$(\text{Ph}_4\text{P})_2\text{IC}_{60}$ contains singly charged fulleride anions, with nearly isolated C_{60}^- anions in the solid state environment due to the large-sized cation (see Fig. 1). The infrared transmittance and absorbance spectra of $(\text{Ph}_4\text{P})_2\text{IC}_{60}$ are presented in Fig. 3 between 300 and 20000 cm^{-1} at room temperature. A small region of the spectrum is cut out between $2000\text{--}4000 \text{ cm}^{-1}$ due to multiphonon absorption in the diamond anvils. The vibrational modes are observed in the far- and mid-infrared region, whereas the electronic transitions appear in the NIR-visible region between $6000\text{--}12000 \text{ cm}^{-1}$ (see inset of Fig. 3). The frequency positions, relative strengths, and assignments of the vibrational modes are listed in Table I.

It is apparent from the infrared spectrum of $(\text{Ph}_4\text{P})_2\text{IC}_{60}$ that it contains numerous vibrational modes of C_{60}^- and of the $(\text{Ph}_4\text{P}^+)_2\text{I}$ cation in the FIR and MIR region. In order to illustrate the contribution of the cation to the richness of the $(\text{Ph}_4\text{P})_2\text{IC}_{60}$ vibrational spectrum, Fig. 4 shows the infrared absorbance spectrum of $(\text{Ph}_4\text{P})_2\text{IC}_{60}$ (at 0.1 GPa) in comparison with that of pure $(\text{Ph}_4\text{P})_2\text{I}$ at ambient conditions.

We first focus on the four fundamental T_{1u} modes of C_{60}^- and the electronic transitions observed in the lowest-pressure absorbance spectrum of $(\text{Ph}_4\text{P})_2\text{IC}_{60}$, as depicted in Figs. 5 and 6, respectively. Neutral C_{60} has a triply degenerate, empty LUMO (lowest unoccupied molecular orbital) and a completely filled HOMO (highest occupied molecular orbital)

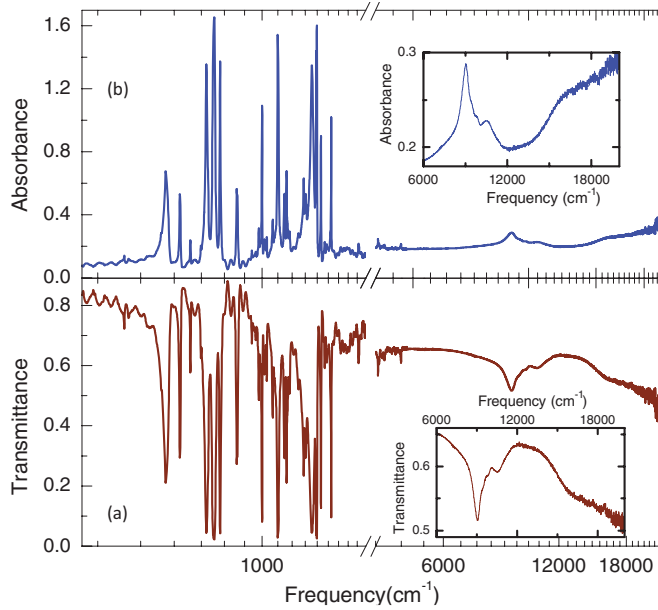


FIG. 3. (Color online) (a) Infrared transmittance and (b) corresponding absorbance spectra of $(\text{Ph}_4\text{P})_2\text{IC}_{60}$ in the frequency range $300\text{--}20000\text{ cm}^{-1}$ at 0.6 GPa . Insets: Transmittance and absorbance spectra in the NIR-visible region.

(see Fig. 7). When the C_{60} molecule is doped with electrons, the symmetry is lowered depending on the number of electrons added. The LUMO of C_{60} can be occupied by up to six electrons. Such addition of electrons to the C_{60} molecule causes a disturbance in the spherical distribution of the electron

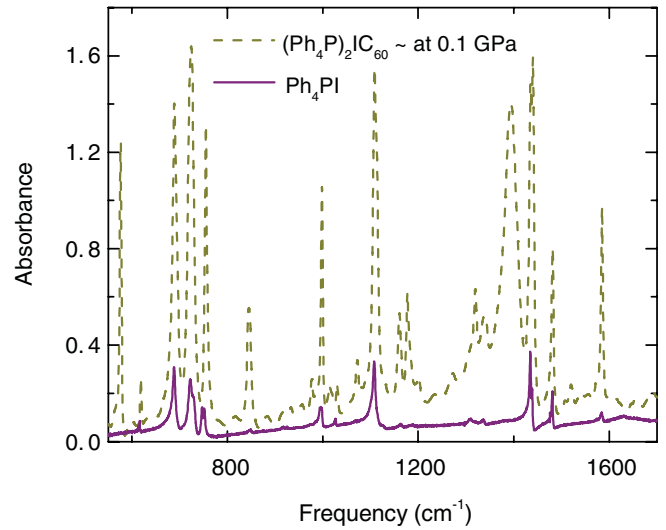


FIG. 4. (Color online) Infrared absorbance spectrum of $(\text{Ph}_4\text{P})_2\text{IC}_{60}$ at $\sim 0.1\text{ GPa}$ and of pure $(\text{Ph}_4\text{P})_2\text{I}$ at ambient pressure.

cloud. In case of C_{60}^- , the additional electron causes a change in the C–C and C=C bonds near the poles. Such stretched bonds are nearly in the direction of the symmetry axis; therefore the spherical C_{60} becomes ellipsoidal C_{60}^- .²² This in turn induces the JT distortion, causing the splitting of the LUMO levels. The JT effect depends on the number of charges added to the C_{60} . It can induce new electronic transitions, shifts, and splittings of the T_{1u} modes, and can lead to the activation of new modes in the vibrational spectra.

TABLE I. Vibrational modes of $(\text{Ph}_4\text{P})_2\text{IC}_{60}$ with their pressure dependence and assignment. The assignments provided are those of the parent mode in C_{60} with I_h symmetry. The strength of the modes is specified as strong (s), medium (m), and weak (w).

Mode Position (at $\sim 0.1\text{ GPa}$) (cm^{-1})	Pressure Dependence	Strength	Assignment
398	hardens, doublet above 2 GPa	w	$G_u(1)$
509	softens	w	
525	hardens	s	cation
517, 533	doublet, hardens	m, s	$T_{1u}(1)$
576, 578	doublet, hardens	s, m	$T_{1u}(2)$
619	hardens, doublet above 2 GPa	w	cation
665	sharpens, hardens, doublet $\sim 2\text{ GPa}$	w	
689, 695	doublet, hardens	s, m	cation
721, 726	doublet, hardens, triplet above 2 GPa	s, s	cation
756	slope change above 2 GPa	s	cation
844, 848	doublet, hardens	w, w	C_{60}^-
975	gains intensity, hardens	w	cation
998	doublet above 2 GPa, hardens	m	cation
1072	hardens	w	C_{60}^-
1108, 1114	doublet, hardens	s, s	
1177, 1182	doublet, hardens	w, w	$T_{1u}(3)$
1201	hardens, undetectable above 3 GPa	w	
1320	hardens, doublet at very high pressure	w	cation
1364, 1395	doublet at low pressure; hardens	w, s	$T_{1u}(4)$
1435, 1440	hardens, doublet	s, s	cation
1482	hardens, doublet above 2 GPa	m	cation
1585	hardens, sharp up to high pressure	m	cation
3047, 3056, 3076, 3088	multiplet, hardens	m, s, w, w	

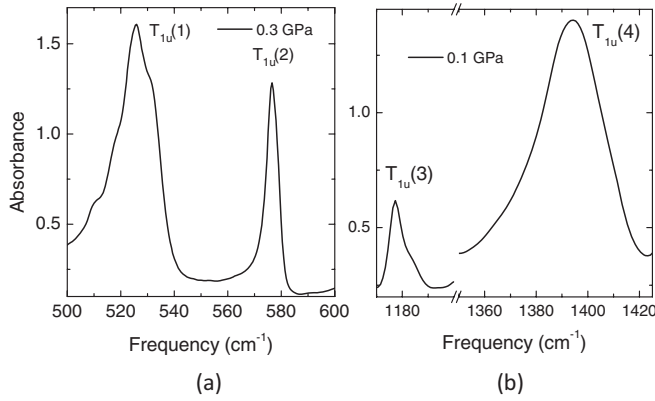


FIG. 5. T_{1u} modes of C_{60}^- at the lowest applied pressure.

The T_{1u} modes of C_{60} are governed by the electron-phonon coupling depending on the charge added to the C_{60} molecules. At room temperature the T_{1u} vibrational modes in neutral C_{60} are sharp singlets resonating at 527, 576, 1182, and 1428 cm^{-1} ,²³ whereas the T_{1u} modes of C_{60}^- in $(\text{Ph}_4\text{P})_2\text{IC}_{60}$ are doublets with the frequencies (1) 517, 533, (2) 576, 578, (3) 1177, 1182, and (4) 1364, 1395 cm^{-1} . At the lowest measured pressure all four T_{1u} modes are split into doublets (see Fig. 5). All the T_{1u} modes except $T_{1u}(2)$ show a redshift compared to C_{60} ,²⁴ attributed to the coupling of the vibrational mode to virtual $t_{1u} \rightarrow t_{1g}$ transitions²⁵ (see scheme in Fig. 7). Furthermore, the T_{1u} modes show strong enhancement of the line width and oscillator strength, and also a change in line shape. Doublet splitting of the T_{1u} modes of the C_{60}^- anion is the signature of the JT effect in the molecule. The room temperature dynamic JT distortion in $(\text{Ph}_4\text{P})_2\text{IC}_{60}$ was also reported by FIR studies.^{5,6} Among these four fundamental vibrational modes, the $T_{1u}(4)$ mode shows the strongest redshift¹⁸ compared to the neutral C_{60} . Furthermore there are silent fullerene modes which become infrared active in $(\text{Ph}_4\text{P})_2\text{IC}_{60}$ due to symmetry lowering, such as the $G_u(1)$ mode at 398 cm^{-1} . The infrared-active cation phonon modes contribute to the richness of the absorbance spectrum as well.

The doublet splitting of the $T_{1u}(1)$ and $T_{1u}(2)$ modes found in our lowest-pressure data is consistent with an earlier report.⁵ Long *et al.*⁵ studied the temperature dependence of vibrational modes and found anomalies in the shift of the frequency positions in the temperature range 125–150 K. For example, the $G_u(1)$ mode at 398 cm^{-1} is reported as a singlet at room temperature and undergoes a doublet splitting during cooling below 150 K. The vibrational mode observed by Long *et al.*⁵ at 504 cm^{-1} , which softens on lowering the temperature, is shifted to 509 cm^{-1} in our data. Besides, the vibrational mode at 619 cm^{-1} only shows a minute frequency shift on lowering the temperature and flattens out below 125 K. The temperature dependence of the vibrational modes will be compared to our pressure-dependent results presented in Sec. III B.

In C_{60}^- the electronic states are coupled to vibrational modes, which gives rise to vibronic transitions. The electronic and vibronic transitions are clearly observed between 6000–12000 cm^{-1} in the NIR region in Fig. 3. For better lucidity the NIR-visible region is presented in the inset. Figure 6 shows the electronic transition in the NIR-visible region of

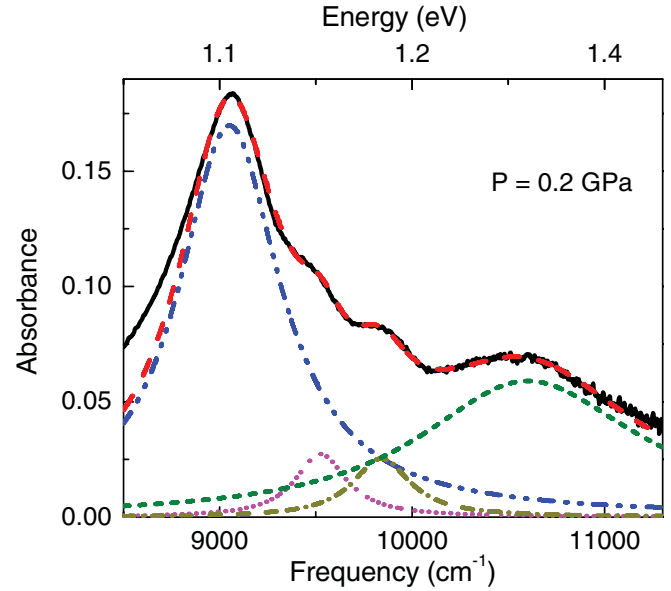


FIG. 6. (Color online) Absorbance spectrum of $(\text{Ph}_4\text{P})_2\text{IC}_{60}$ at 0.2 GPa in the NIR region together with the fit (red dashed line) and its Lorentz oscillator contributions.

the spectrum with the four contributions obtained from the fitting with Lorentz oscillators. To obtain a very good fit on the low-frequency side an additional oscillator is required for describing the background, which does not affect the frequency positions of the other main oscillators representing the electronic transitions. Besides the prominent feature at $\sim 9050 \text{ cm}^{-1}$, three absorption bands between 9300 and 11000 cm^{-1} are observed.

Several NIR investigations report similar spectra on C_{60}^- in solution²⁷ and isolated C_{60}^- .²⁸ Electronic transitions of isolated C_{60}^- in neon matrices showed well-resolved spectra.²⁹ The environment in which the C_{60}^- anion is investigated is an important criterion to determine the nature of the distortion which can either be static or dynamic. On the one hand, C_{60} anions in the solid state are influenced by Coulomb interactions with the cations. On the other hand, even in dilute solutions the influence of the environment can be significant.

In the following, we discuss the four distinct transitions in the NIR-visible region of the spectrum with the help of the transition scheme in Fig. 7. This scheme is based on the splitting of the t_{1u} and t_{1g} LUMO energy levels, whose degeneracy is lifted in C_{60}^- because of the JT distortion and the related symmetry lowering. According to theoretical investigations, the symmetry for C_{60}^- gives rise to the three possible point groups D_{5d} , D_{3d} , or D_{2h} , which possess nearly the same JT energies.²² On an adiabatic potential energy surface there are 6 equivalent structures possible for D_{5d} minima, 10 for D_{3d} minima, and 15 for D_{2h} minima.²² Due to the equivalent energy the dynamic transformation among these distortions can take place. In case of D_{5d} symmetry, the orbitals (${}^2t_{1u}$ and ${}^2t_{1g}$) undergo a doublet splitting into (${}^2a_{2u}$, ${}^2e_{1u}$) and (${}^2e_{1g}$, ${}^2a_{2g}$), respectively, while for D_{3d} it would be (${}^2a_{2u}$, 2e_u) and (2e_g , ${}^2a_{2g}$), respectively. The splitting of the energy levels is illustrated in Fig. 7. For both D_{5d} and D_{3d} symmetry reduction a single optically allowed transition of the form $a_{2u} \rightarrow e_g$ is expected (see Fig. 7). The different

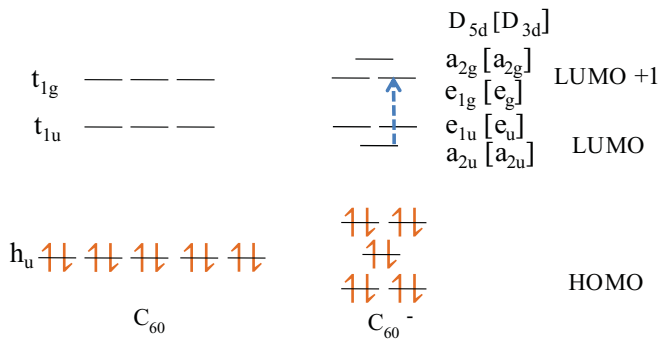


FIG. 7. (Color online) Illustration of molecular orbitals of C_{60} and C_{60}^- for D_{5d} [D_{3d}] symmetry according to Refs. 26,31. The blue dotted line indicates the optically allowed transition in C_{60}^- .

orientations for D_{5d} and D_{3d} distortions are separated by shallow energy minima which are connected by pseudorotation causing the disorder in the dynamic system. In case of D_{2h} symmetry, the ${}^2t_{1u}$ and ${}^2t_{1g}$ levels undergo a triplet splitting into (${}^2b_{1u}$, ${}^2b_{2u}$, ${}^2b_{3u}$) and (${}^2b_{1g}$, ${}^2b_{2g}$, ${}^2b_{3g}$), respectively. Thus, a D_{2h} distortion of the fullerene molecule would give rise to two optically allowed transitions of the type $b_{1u} \rightarrow b_{3g}$ and $b_{1u} \rightarrow b_{2g}$.²⁷ It has been suggested that the D_{2h} symmetry can be stabilized only in a crystal field, but not in the case of a free C_{60} .³⁰ The possibility of D_{2h} symmetry for C_{60}^- has been ruled out due to the narrow line in the FIR spectrum reported earlier.⁵

According to Lawson *et al.*²⁶ the features in the NIR region are due to the symmetry reduction to D_{5d} of the isolated C_{60}^- anion investigated in benzonitrile solution. The strong feature at 1078 nm (9276 cm^{-1}) in the spectrum is attributed to the optically allowed $a_{2u} \rightarrow e_{1g}$ transition which is in accordance with the density functional calculations by

Green *et al.*³¹ The manifold around 800–1000 nm ($10000\text{--}12500\text{ cm}^{-1}$), which is not very well resolved in Ref. 26, is assigned to the vibronic transitions to the level a_{2g} . In a recent NIR investigation on C_{60}^- carried out by Hands *et al.*,³² a well-resolved spectrum in the region $9000\text{--}13000\text{ cm}^{-1}$ is presented. They discuss the possibility of D_{3d} and D_{5d} symmetry and claim that the four contributions in the NIR region are due to the D_{3d} symmetry, and that the spectrum would have fewer contributions in case of D_{5d} symmetry. The C_{60}^- ion prepared in other media such as in a gas matrix,²⁹ by electrogeneration,³³ and in salts³⁴ was also studied at ambient conditions. Also theoretical calculations^{22,35} have been carried out to explain the complicated electronic transition observed in C_{60}^- . Hands *et al.*³⁵ state that the dynamics for a minimum of D_{5d} symmetry is simpler than that of D_{3d} due to the tunneling splitting between symmetry-adapted states that correctly describe tunneling between equivalent minima. Obviously, there are alternative explanations for the results reported in Ref. 26.

According to the above described earlier theoretical and experimental results, we interpret our NIR absorbance spectrum for the lowest pressure in terms of a C_{60}^- molecule dynamically fluctuating between D_{3d} and D_{5d} symmetry. Within this picture, the t_{1u} and t_{1g} (LUMO and LUMO + 1, respectively) levels are split into two levels^{31,35} (see scheme in Fig. 7). We interpret the NIR spectrum as the combination of electronic and manifold vibronic transitions. The prominent feature at 9049.8 cm^{-1} is due to the optically allowed $a_{2u} \rightarrow e_{1g}$ transition either in D_{5d} or D_{3d} symmetry. The manifold between 9300 and 11000 cm^{-1} is due to vibronic transitions. Based on our FIR-MIR data and earlier results⁵ we suggest that the symmetry of C_{60}^- near ambient conditions is governed by the dynamic JT effect (presumably of D_{3d} and D_{5d} symmetry). However, a further symmetry lowering, for example from D_{5d}

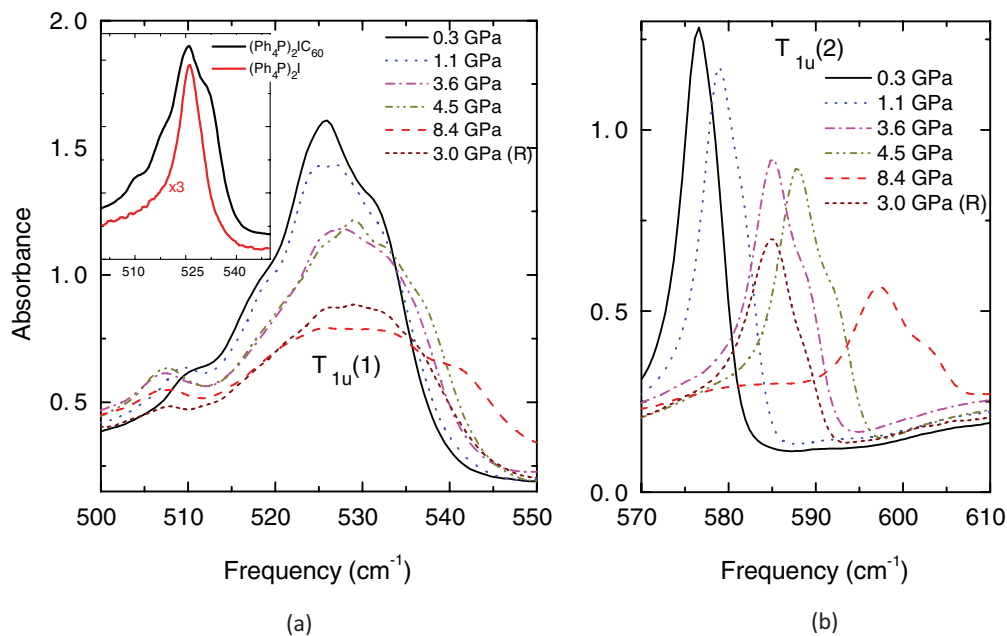


FIG. 8. (Color online) (a) $T_{1u}(1)$ and (b) $T_{1u}(2)$ infrared absorbance spectra of $(\text{Ph}_4\text{P})_2\text{IC}_{60}$ for various pressures. Inset: Comparison of the absorbance spectra of $(\text{Ph}_4\text{P})_2\text{IC}_{60}$ and $(\text{Ph}_4\text{P})_2\text{I}$ between 500 and 550 cm^{-1} . The label (R) indicates the spectra measured during pressure release.

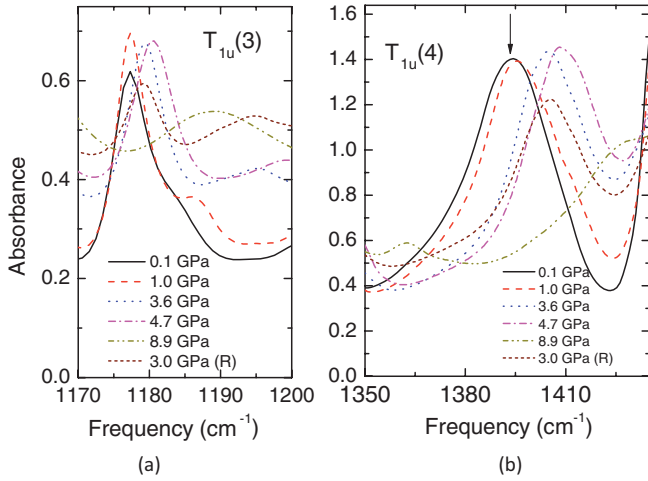


FIG. 9. (Color online) (a) $T_{1u}(3)$ and (b) $T_{1u}(4)$ infrared absorbance spectrum of $(\text{Ph}_4\text{P})_2\text{IC}_{60}$. The $T_{1u}(4)$ mode is marked with an arrow. The label (R) indicates the spectra measured during pressure release.

to C_{2h} or C_i , cannot be ruled out, as pointed out recently in the case of $(\text{Ph}_4\text{As})_2\text{ClC}_{60}$.⁷

B. Pressure dependence of vibrational modes and electronic transitions of $(\text{Ph}_4\text{P})_2\text{IC}_{60}$

Next we will focus on the effect of pressure on the vibrational and electronic excitations in $(\text{Ph}_4\text{P})_2\text{IC}_{60}$. For a quantitative analysis, the frequency positions of the vibrational modes were extracted by fitting the modes with Lorentzian functions. The pressure dependence of all modes is summarized in Table I. Figures 8 and 9 show the four fundamental T_{1u} vibrational modes of C_{60}^- for selected pressures. The $T_{1u}(1)$ is strongly overlapped by a counterion mode, as illustrated in the inset of Fig. 8(a). Also the $(\text{Ph}_4\text{P})^+$ cation modes undergo pressure-induced changes [see Fig. 8(a)]; this complicates the

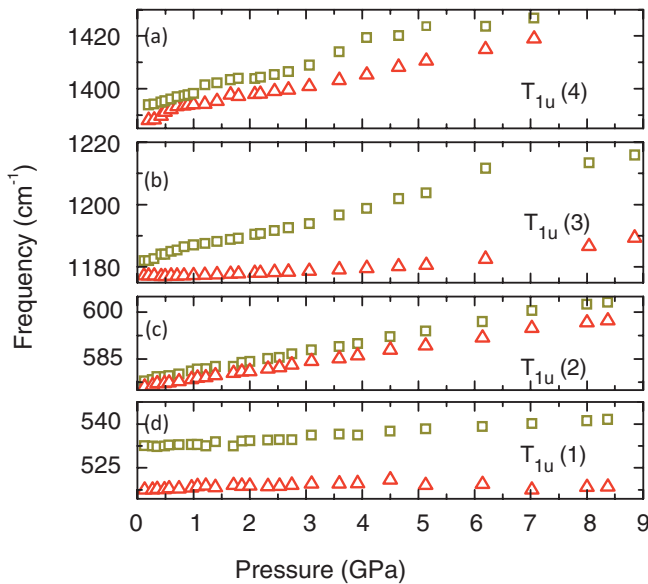


FIG. 10. (Color online) Frequency positions of the T_{1u} vibrational modes as a function of pressure.

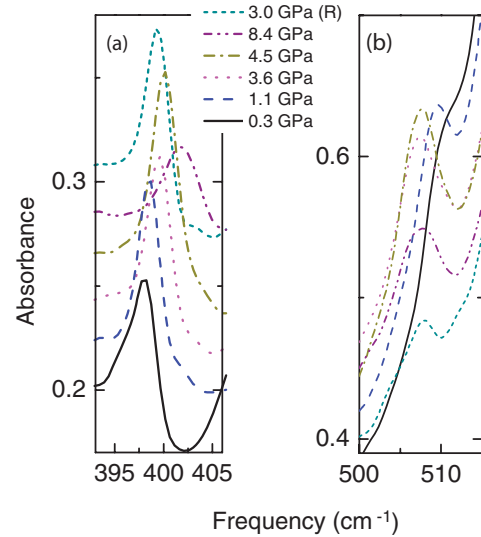


FIG. 11. (Color online) Absorbance spectra of the vibrational modes of $(\text{Ph}_4\text{P})_2\text{IC}_{60}$ in the FIR region for various pressures (shifted for clarity). The label (R) indicates the spectra measured during pressure release.

analysis of this mode. The pressure-dependent frequencies of T_{1u} vibrational modes are plotted in Fig. 10. It is evident that all the T_{1u} modes are split into doublets at near-ambient conditions and harden with increasing pressure. We do not observe any anomaly in the pressure dependence of their frequency positions, in contrast to the findings as a function of temperature.⁵ Figure 12(a) shows the pressure dependence of the cation modes at around 518 cm^{-1} , close to the $T_{1u}(1)$ mode's position.

The other prominent vibrational modes in the FIR region are the $G_u(1)$ mode at 398 cm^{-1} , depicted in Fig. 11(a) for various pressures, and another mode at 509 cm^{-1} [see Fig. 11(b)], whose assignment is not clear. The frequency positions of these modes are plotted as a function of pressure in Figs. 12(b) and 12(c). The $G_u(1)$ mode is a singlet at low pressure,

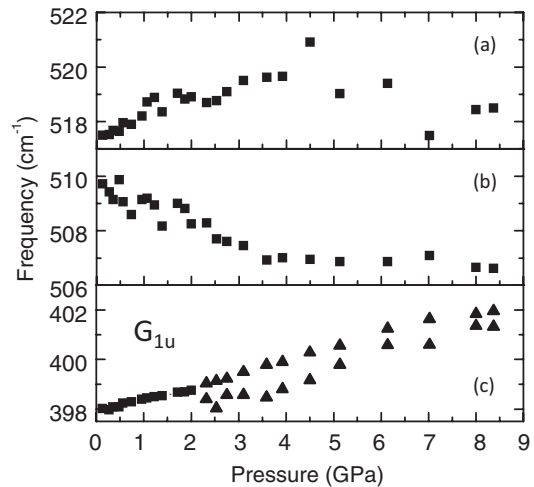


FIG. 12. Pressure dependence of the frequency positions of the cation modes close to the $T_{1u}(1)$ mode [(a) and (b)] and of the G_{1u} vibrational mode (c).

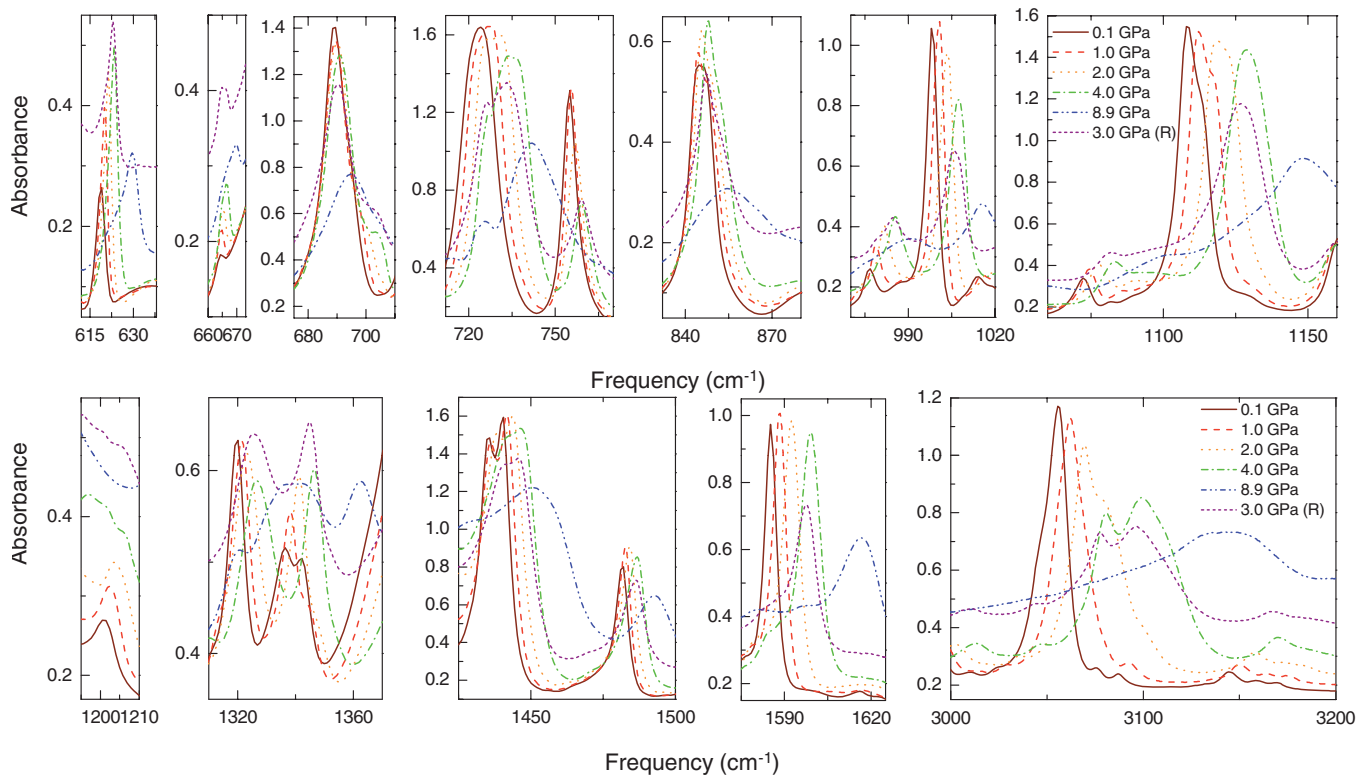


FIG. 13. (Color online) Absorbance spectra of the vibrational modes of $(\text{Ph}_4\text{P})_2\text{IC}_{60}$ in the MIR region for various pressures. The label (R) indicates the spectra measured during pressure release.

hardens with increasing pressure, and becomes a doublet above 2 GPa [see Fig. 12(c)]. This behavior is consistent with the temperature-dependent results of $(\text{Ph}_4\text{P})_2\text{IC}_{60}$ where the $G_u(1)$ undergoes a twofold splitting at 150 K while cooling down from room temperature.⁵ According to group theory, a twofold splitting of the G_u mode is expected as the system settles for a lower symmetry. The vibrational mode at 509 cm^{-1} is one of the few modes which soften with increasing pressure, which is also consistent with the behavior during temperature decrease. The intensity of this mode steadily increases with increasing pressure and remains sharp until the highest pressure applied.

Figure 13 shows the evolution of the absorbance spectrum with increasing pressures for various vibrational modes observed in the mid-infrared region of the spectrum. There are numerous modes in this range, and we will discuss the prominent ones in detail in this section. Their pressure dependence is included in Table I. Figures 14 and 15 show the pressure-dependent frequency position of the MIR vibrational modes: All the modes show a hardening behavior with increasing pressure. The vibrational mode at 619 cm^{-1} is a singlet at the lowest pressure and undergoes a doublet splitting at pressures above 2 GPa. In contrast, by lowering the temperature at ambient pressure no splitting of this mode occurs. This mode is attributed to the cation. The vibrational mode at 665 cm^{-1} is attributed to the C_{60}^- .⁷ It is a weak mode but gains intensity and remains sharp up to high pressure, and also shows a twofold splitting on increasing pressure above 2 GPa. There are several vibrational modes observed due to the cation between 680 and 3150 cm^{-1} in the MIR region. The vibrational

mode around 720 cm^{-1} is a cation mode and is a doublet at the lowest pressure; above 2 GPa it transforms to a threefold mode. The twofold vibrational mode around 846 cm^{-1} might be attributed to the C_{60}^- vibration.⁷ The vibrational mode at 1482 cm^{-1} is a singlet at low pressure and undergoes a twofold splitting above 2 GPa. The vibration around 3050 cm^{-1} is an intense doublet which is followed by weak modes on the high-energy side at 3076 and 3088 cm^{-1} . The influence of pressure on this multiplet has different pressure coefficients. The weak modes on the higher energy side cannot be observed at higher pressures. In the frequency versus pressure plot shown in Fig. 15 there appears to be a crossing over of the vibrational mode around 1 GPa. This is mainly due to different pressure coefficients of the modes; unfortunately, the origin of these modes is not clear.

The observed splitting of several vibrational modes is an indication of a change in symmetry. Several FIR and MIR vibrational modes show a splitting above 2 GPa. This can be understood as the molecule exhibits dynamic distortions at near-ambient conditions with either D_{5d} or D_{3d} symmetry. When there is dynamic JT effect on the time scale of the IR measurement, then the symmetry is averaging out during the lifetime of one excitation, and therefore IR spectroscopy sees higher apparent symmetry. On application of hydrostatic pressure, the fulleride ions are “squeezed,” which prevents the pseudorotation of the molecule from one distortion to the other; therefore it stays in one specific distortion beyond a critical pressure. The lower symmetry (D_{3d} or lower in our case) is determined by the environment provided by the cation and causes the splitting of the vibrational modes. The critical

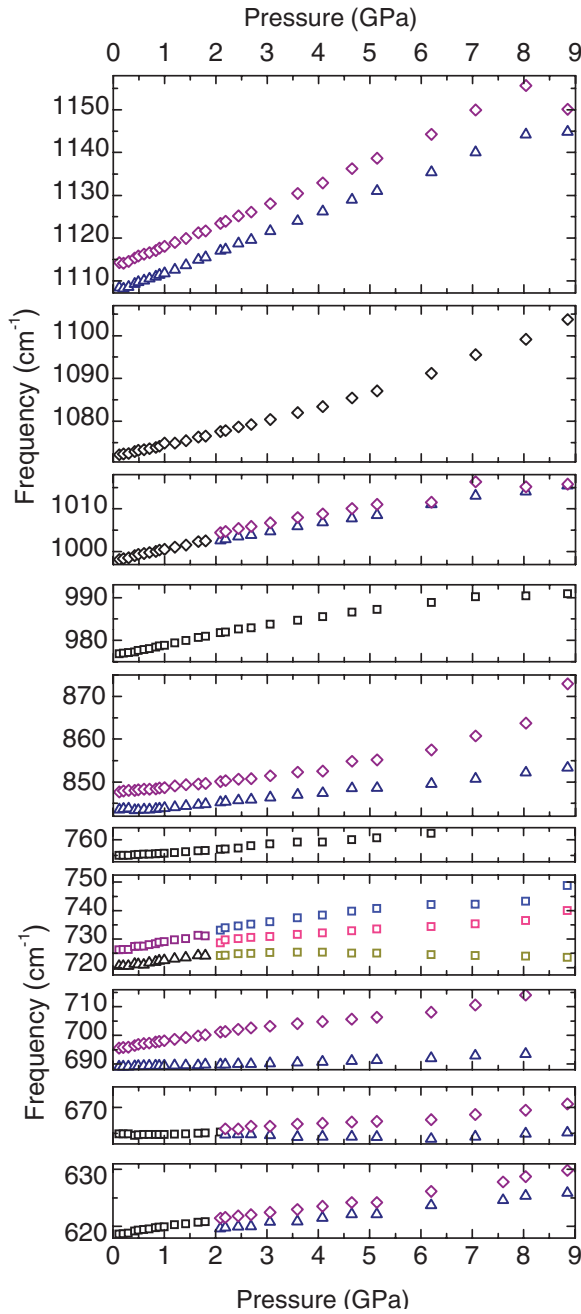


FIG. 14. (Color online) Frequency positions of the vibrational modes of $(\text{Ph}_4\text{P})_2\text{IC}_{60}$ as a function of pressure.

pressure of the transition to the static state is around 2 GPa. We speculate here that the dynamic-to-static transition induced by external pressure is analogous to the observed transition at around 150 K,⁷ the driving force being the cation-anion interaction (steric crowding).

The NIR-visible absorbance spectrum of $(\text{Ph}_4\text{P})_2\text{IC}_{60}$ is shown in Fig. 16 for selected pressures. The bands between 9000 cm^{-1} and 12000 cm^{-1} correspond to electronic and vibronic excitations of the C_{60}^- anion, as discussed in Sec. III A. With increasing pressure they shift to lower energies; the shifts are reversible upon pressure release. The redshift of the transitions is clearer in Fig. 17, where the frequency positions of the bands, as extracted from Lorentz fitting, are plotted as

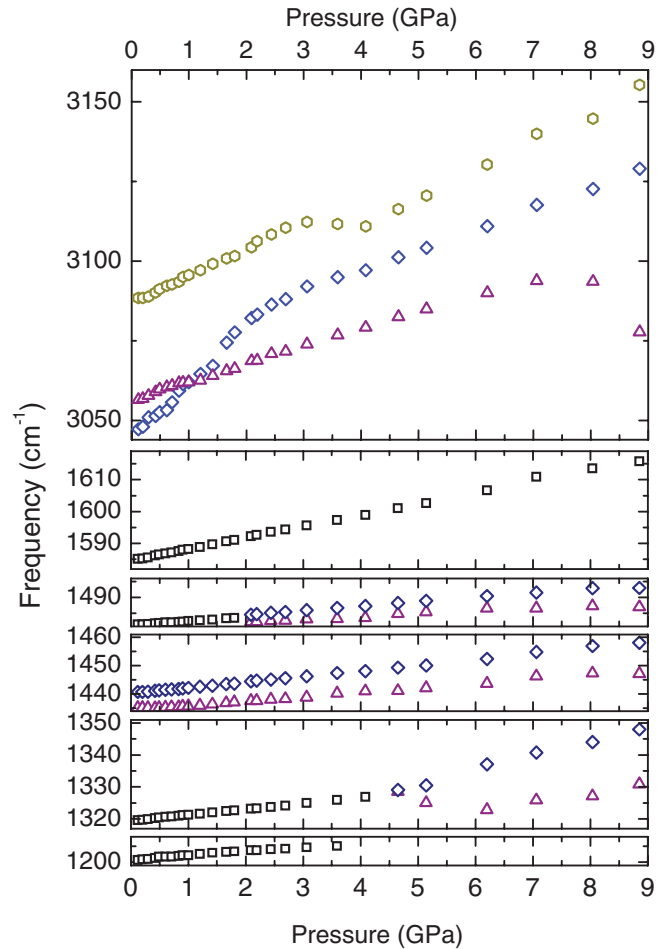


FIG. 15. (Color online) Frequency positions of various vibrational modes of $(\text{Ph}_4\text{P})_2\text{IC}_{60}$ as a function of pressure.

a function of pressure. Since the feature around 9450 cm^{-1} and 9700 cm^{-1} broadens considerably at high pressure, the error bar is larger above 4 GPa compared to the lower-pressure

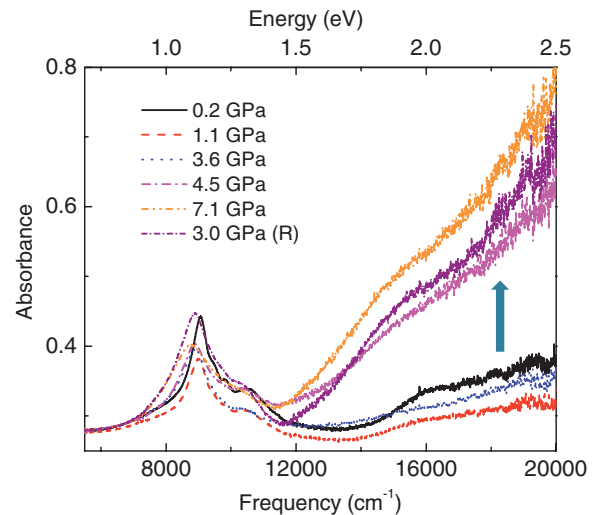


FIG. 16. (Color online) Infrared absorbance spectrum of $(\text{Ph}_4\text{P})_2\text{IC}_{60}$ in the NIR-visible region for various pressures. The label (R) indicates the spectra measured during pressure release.

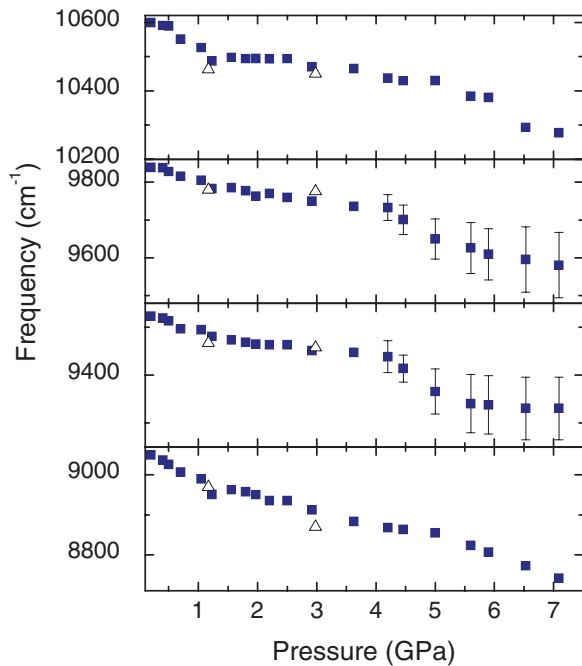


FIG. 17. (Color online) Frequency positions of the electronic excitations of C_{60}^- in $(Ph_4P)_2IC_{60}$ as a function of pressure. At higher pressures the error bars are enlarged because of the broadening of the transitions. Open triangles indicate the results for releasing pressure.

regime. The softening of the electronic and vibronic transitions could be due to the fact that the compression of the lattice produced by the applied pressure reduces the splitting of the electronic states. The absorption in the visible region of the spectrum above 12000 cm^{-1} abruptly increases for pressures above $\approx 4\text{ GPa}$ (see Fig. 16). Higher-energy data would be

needed in order to clearly trace the details of this change as a function of pressure. The pressure-induced changes on this high-energy transition are irreversible above 5 GPa according to our results.

IV. SUMMARY

In summary, we have studied the pressure dependence of the vibrational and electronic/vibronic excitations in $(Ph_4P)_2IC_{60}$ by infrared transmission measurements up to 9 GPa over a broad frequency range ($200\text{--}20000\text{ cm}^{-1}$). The four fundamental T_{1u} modes of C_{60}^- are split into a doublet already at the lowest applied pressure and harden with increasing pressure. Several cation modes and fullerene-related modes split into a doublet at around 2 GPa, the most prominent one being the G_{1u} mode of fullerene. We interpret these mode splittings in terms of the transition from the dynamic to static Jahn-Teller effect. Four absorption bands are observed in the NIR-visible frequency range, which correspond to excitations between t_{1u} and t_{1g} LUMO energy levels, split due to the Jahn-Teller distortion. The optically allowed $a_{2u} \rightarrow e_{1g}$ transition (either in D_{5d} or D_{3d} symmetry) and the three energetically higher-lying vibronic transitions shift to lower energies with increasing pressure, indicating a reduction of the splitting of the LUMO electronic states under pressure application.

ACKNOWLEDGMENTS

We gratefully acknowledge financial support by the German Science Foundation (DFG) and the Hungarian Academy of Sciences under Cooperation Grant No. DFG/183, and the Hungarian National Research Fund (OTKA) under Grant No. 75813.

*christine.kuntscher@physik.uni-augsburg.de

- ¹J. L. Sauvajol, A. Graja, L. Firlej, and S. Król, *J. Mol. Struct.* **436**, 19 (1997).
- ²K. Pilz, A. Jobst, E. Lam, J. Lüdecke, J. Bao, W. Bietsch, and M. Schwoerer, *Z. Kristallogr.* **217**, 78 (2002).
- ³A. Penicaud, A. Perez-Benitez, V. R. Gleason, P. E. Munoz, and R. Escudero, *J. Am. Chem. Soc.* **115**, 10390 (1993).
- ⁴U. Bilow and M. Jansen, *Z. Anorg. Allg. Chem.* **621**, 982 (1995).
- ⁵V. C. Long, J. L. Musfeldt, K. Kamarás, A. Schilder, and W. Schütz, *Phys. Rev. B* **58**, 14338 (1998).
- ⁶V. C. Long, J. L. Musfeldt, K. Kamarás, A. Schilder, and W. Schütz, *Synth. Met.* **103**, 2435 (1999).
- ⁷V. C. Long, E. C. Schundler, G. B. Adams, J. B. Page, W. Bietsch, and I. Bauer, *Phys. Rev. B* **75**, 125402 (2007).
- ⁸B. Gotschy, M. Keil, H. Klos, and I. Rystau, *Solid State Commun.* **92**, 935 (1994).
- ⁹B. Gotschy and G. Völkel, *Appl. Magn. Reson.* **11**, 229 (1996).
- ¹⁰G. Völkel, A. Pöpl, J. Simon, J. Hoentsch, S. Orlinskii, H. Klos, and B. Gotschy, *Phys. Rev. B* **52**, 10188 (1995).
- ¹¹U. Becker, G. Denninger, V. Dyakonov, B. Gotschy, H. Klos, G. Rosler, A. Hirsch, and H. Winter, *Europhys. Lett.* **21**, 267 (1993).

- ¹²W. Bietsch, J. Bao, J. Lüdecke, and S. van Smaalen, *Chem. Phys. Lett.* **324**, 37 (2000).
- ¹³P. Launois, R. Moret, N-R. De Souza, J. A. Azamar-Barrios, and A. Penicaud, *Eur. Phys. J. B* **15**, 445 (2000).
- ¹⁴E. A. Francis, S. Scharinger, K. Németh, K. Kamarás, and C. A. Kuntscher, *Phys. Status Solidi B* **247**, 3047 (2010).
- ¹⁵B. Sundqvist, *Adv. Phys.* **48**, 1 (1999).
- ¹⁶K. Thirunavukkuarasu, C. A. Kuntscher, Gy. Bényei, I. Jalsovszky, G. Klupp, K. Kamarás, É. Kováts, and S. Pekker, *Phys. Status Solidi B* **244**, 3857 (2007).
- ¹⁷K. Thirunavukkuarasu, C. A. Kuntscher, B. J. Nagy, I. Jalsovszky, G. Klupp, K. Kamarás, É. Kováts, and S. Pekker, *J. Phys. Chem. C* **112**, 17525 (2008).
- ¹⁸V. N. Semkin, N. G. Spitsina, S. Król, and A. Graja, *Chem. Phys. Lett.* **256**, 616 (1996).
- ¹⁹P. M. Allemand, G. Srdanov, A. Koch, K. Khemani, and F. Wudl, *J. Am. Chem. Soc.* **113**, 2780 (1991).
- ²⁰G. Huber, K. Syassen, and W. B. Holzapfel, *Phys. Rev. B* **15**, 5123 (1977).
- ²¹H. K. Mao, J. Xu, and P. M. Bell, *J. Geophys. Res.* **91**, 4673 (1986).
- ²²N. Koga and K. Morokuma, *Chem. Phys. Lett.* **196**, 191 (1992).

- ²³W. Krätschmer, L. D. Lamb, K. Forstiropoulos, and D. R. Huffman, *Nature (London)* **347**, 354 (1990).
- ²⁴T. Pichler, R. Winkler, and H. Kuzmany, *Phys. Rev. B* **49**, 15879 (1994).
- ²⁵M. J. Rice and H.-Y. Choi, *Phys. Rev. B* **45**, 10173 (1992).
- ²⁶D. R. Lawson, D. L. Feldheim, C. A. Foss, P. K. Dorhout, C. M. Elliott, C. R. Martin, and B. Parkinson, *J. Electrochem. Soc.* **139**, 7 (1992).
- ²⁷H. Kondo, T. Momose, and T. Shida, *Chem. Phys. Lett.* **237**, 111 (1995).
- ²⁸S. Tomita, J. U. Andersen, E. Bonderup, P. Hvelplund, B. Liu, S. B. Nielsen, U. V. Pedersen, J. Rangama, K. Hansen, and O. Echt, *Phys. Rev. Lett.* **94**, 053002 (2005).
- ²⁹J. Fulara, M. Jakobi, and J. P. Maier, *Chem. Phys. Lett.* **211**, 227 (1993).
- ³⁰C. C. Chancey and M. C. M. O'Brien, *The Jahn-Teller Effect in C₆₀ and Other Icosahedral Complexes* (Princeton University Press, Princeton, NJ, 1997).
- ³¹W. H. Green, S. M. Gorun, G. Fitzgerald, P. W. Fowler, A. Ceulemans, and B. C. Titeca, *J. Phys. Chem.* **100**, 14892 (1996).
- ³²I. D. Hands, J. L. Dunn, C. A. Bates, M. J. Hope, S. R. Meech, and D. L. Andrews, *Phys. Rev. B* **77**, 115445 (2008).
- ³³G. A. Heath, J. E. McGrady, and R. L. Martin, *J. Chem. Soc. Chem. Commun.* **17**, 1272 (1992).
- ³⁴R. D. Bolskar, S. H. Gallagher, R. S. Armstrong, P. A. Lay, and C. A. Reed, *Chem. Phys. Lett.* **247**, 57 (1995).
- ³⁵I. D. Hands, J. L. Dunn, and C. A. Bates, *Phys. Rev. B* **73**, 235425 (2006).